Journal of Power Sources 196 (2011) 2202–2210

Contents lists available at ScienceDirect

Journal of Power Sources

journal homepage: www.elsevier.com/locate/jpowsour

# Preparation and ion transport properties of NaY zeolite–ionic liquid composites

S. Ntais[a], A.M. Moschovi[b], F. Paloukis[a], S. Neophytides[a], V.N. Burganos[a], V. Dracopoulos[a], V. Nikolakis[a,*]

[a] Foundation for Research and Technology Hellas, Institute of Chemical Engineering and High Temperature Chemical Processes, Stadiou str, Platani, P.O. Box 1414, GR 26504, Rio Patras, Greece
[b] Department of Chemical Engineering, University of Patras, 26504 Patras, Greece

ARTICLE INFO

*Article history:*
Received 22 July 2010
Received in revised form
16 September 2010
Accepted 21 September 2010
Available online 29 September 2010

*Keywords:*
Fuel cells
PEM membranes
Ionic liquids
Zeolites
Effective Medium Theory
Conductivity

ABSTRACT

The physicochemical properties of protic ionic liquids (IL)–zeolite (Z) composites were investigated. H-3 methylimidazolium bis(trifluoromethanesulfonyl) imide (TFSI)/NaY zeolite composites with different IL/Z weight ratios were prepared and characterized. X-ray diffraction and FT-Raman measurements show the formation of NaTFSI during the preparation procedure which indicates that an ion exchange reaction is taking place during the composite preparation method. $N_2$ physisorption shows that the zeolite pores are completely filled when IL/Z ratio is between 0.2 and 0.5. The water adsorption capacity of the samples decreased with IL/Z ratio. The conductivity of the composite pellets increased with temperature and ionic liquid loading, however significant enhancement was detected once the IL/Z weight ratio was higher than a threshold value (~0.5). Moreover, theoretical calculations were performed using the Effective Medium Theory in order to understand the effect of IL/Z ratio on conductivity. In qualitative agreement with the experimental data, the model shows a sharp increase of the conductivity right above a critical threshold value for the ionic liquid/zeolite mass ratio, followed by a more moderate increase at higher loadings.


## 1. Introduction

Fuel cells (FCs) have been recognized as important devices for efficient transformation of chemical energy to electricity. They have the potential to replace internal combustion engines in vehicles, to produce energy in remote locations or to be part of portable Auxiliary Power Units. Among the different fuel cell types those of Polymer Electrolyte Membranes (PEMs) have received significant attention. In such FCs a membrane that ideally enables only proton transport is the barrier between the anode and cathode. Nafion, which is usually used for this purpose, requires relatively low operating temperatures (<100 °C) in order to maintain the necessary levels of hydration for proton conduction. However, at such low operating temperature, two important drawbacks arise: (i) it is not easy to recover the waste heat; (ii) the Pt catalyst of the electrodes is very sensitive to CO poisoning. To address these issues, intensive efforts are made to develop High Temperature Polymer Electrolyte Membranes (HTPEMs), with operating temperatures up to 200 °C.

The most promising technological application for high temperature PEM fuel cells is based on materials that combine acid–base interactions in order to acquire high proton conductivity ($10^{-1}$ S cm$^{-1}$) at temperatures ranging between 140 °C and 200 °C. Polybenzimidazole (PBI) [1] and aromatic polyethers with pyridine units (TPS) [2] imbibed with phosphoric acid are considered the state of the art high temperature polymer electrolytes, combining high thermal stability with increased proton conductivity. The polymeric membranes are imbibed with phosphoric acid so that the proton acceptor sites of the benzimidazole ring (PBI) and the pyridine units (TPS) interact with the phosphoric acid molecules due to acid–base interactions providing proton conducting materials. Though this technology concentrates several advantages related to the high operating temperature, one of its main drawbacks is the poisoning effect of the phosphoric anions on the oxygen reduction reaction. This can be tackled either by the development of novel phosphoric acid resistant electrocatalysts or the synthesis and development of novel proton conducting electrolyte membranes. Two types of materials that have been proposed to address these issues are microporous oxides, such as zeolites, and protic ionic liquids. Zeolites with low Si/Al ratio are hydrophilic and have the potential to increase the membrane water content at elevated temperatures. Furthermore, if incorporated in a polymer matrix, they might also decrease fuel crossover. Previous studies on zeolites attributed their conduction properties to cation migration [3]. As a result, only proton exchanged zeolites should be able to exhibit the beneficial to PEMs, proton conductivity. However, proton exchanged zeolites were found to have almost two orders of magnitude lower conductivities compared to their $Na^+$ exchanged

* Corresponding author. Tel.: +30 2610965242; fax: +30 2610965223.
*E-mail address:* vnikolak@iceht.forth.gr (V. Nikolakis).

0378-7753/$ – see front matter © 2010 Elsevier B.V. All rights reserved.
doi:10.1016/j.jpowsour.2010.09.061

form [4]. This observation was attributed to the higher interaction of the protons with the oxygen atoms of the framework. Even though the adsorption of water was found to significantly increase ionic conductivity, the maximum values reported are of the order of $\sim 10^{-4}$ S cm$^{-1}$ [5]. Thus, the zeolite poor conductivity is expected to have a negative effect on the overall PEM proton conduction. To address this issue several groups have synthesised and tested acid functionalized mesoporous materials and zeolites [6–10]. In particular, functionalization of zeolites BEA, MCM-48 and MCM-41 with phenethyl sulfonic acid or mercaptopropyl sulfonic acid increased the proton conductivity of the powders approximately two orders of magnitude [7].

Ionic liquids (ILs) are salts with low melting points that are characterized by their enhanced thermal stability, non-volatility and non-flammability. Organic cations with low symmetry such as ammonium, sulfonium and imidazolium are usually combined with polynuclear or mononuclear anions. These properties as well as the essentially unlimited number of potential ILs have attracted the attention of researchers both for fundamental studies as well as for the development of new IL based applications i.e. separation technology [11,12], catalysis [13], electrochemistry [14] etc. Protic ionic liquids are formed by mixing Brønsted acids and bases. It has recently been shown that this type of ILs can undergo hydrogen oxidation and oxygen reduction reactions in the absence of water molecules and, thus, could be used as proton carriers in fuel cells operating in anhydrous conditions [15,16]. Promising results have been reported by Iojoiu et al. [17] who studied the performance of Nafion membranes impregnated by triflate triethylammonium or methane sulfonate triethylammonium protic ionic liquids. Ye et al. [18] studied the proton conduction in composite membranes comprised of polybenzimidazole (PBI), $H_3PO_4$ and the protic IL 1-propyl-3methylimidazolium dihydrogen phosphate ($PMIH_2PO_4$). Finally, Lee et al. [19] tested the performance of sulfonated polyimide membranes that contained diethylmethylammonium trifluoromethanesulfonate as protic ionic liquid. The ionic conductivity of these membranes was more than 10 mS cm$^{-1}$ at 120 °C.

The combination of the two aforementioned types of materials (zeolites and ionic liquids) could result in composite materials suitable for different applications. During the last decade, ionic liquids have been immobilised in porous substrates (e.g. $SiO_2$, $TiO_2$, etc.) or zeolites. DeCastro et al. [20] have immobilised a mixture of 1-butyl-3-methyl-imidazolium chloride and $AlCl_3$ (Al-IL) on different porous supports ($SiO_2$, $Al_2O_3$, $TiO_2$, $ZrO_2$ and H-BEA zeolite) in order to prepare catalysts for the alkylation reactions of aromatic compounds. Valkenberg et al. [21] presented three different approaches for immobilising ILs on zeolites and other porous supports for the preparation of novel catalysts for the Friedel–Crafts reaction. Pietschmann et al. [22] impregnated [EMIM$^+$][$BF_4^-$] in zeolite BEA and mesoporous silica (SBA-15) using "wet impregnation" and a suitable solvent (methanol). The crystals were separated from the suspension using filtration and any excess of IL was removed by Soxhlet extraction.

The goal of most of the previous studies was to combine the properties of the ILs and the microporous materials to design novel catalyst with improved performance. The present work aims to study the encapsulation of a protic IL in zeolite NaY, and to understand its effect on zeolite conduction properties. Such composite materials might become one constituent of a composite membrane for HTPEM fuel cells. H-3-methylimidazolium bis(trifluoromethanesulfonyl) imide (HMITFSI) is selected as the protic IL in this study. The composites are characterized using powder X-ray diffraction and vibrational spectroscopy (FT-Raman). The textural properties and the water capacity of the composites are evaluated using $N_2$ physisorption measurements and TGA. Finally, the electric conductivity of pellets of the synthesised composites was measured using AC impedance spectroscopy.

Such measurements depict the conductivity of the granular system (pellets) and not that of the zeolite particle. To address this issue the Effective Medium Theory (EMT) is used to estimate the zeolite/ionic liquid conductivity at the grain scale as inferred from conductivity measurements at the macroscopic scale. Furthermore, the effect of the distribution of the ionic liquid in the intergranular space, and in the interior of the zeolite grains on the conductivity of the composite material is quantitatively investigated using a modified, two-step EMT approach.

## 2. Experimental

H-3-methylimidazolium bis(trifluoromethanesulfonyl) imide (HMITFSI) 99.5% and sodium bis(trifluoromethanesulfonyl) imide (NaTFSI) were supplied by SOLVIONIC S.A. HMITFSI was stored under Ar in a desiccator and used without further purification. NaY–FAU zeolite was purchased from Sigma–Aldrich.

### 2.1. Ionic liquid encapsulation

The following procedure has been used for the encapsulation of HMITFSI in the zeolite pores: (i) NaY crystals were outgassed for ~24 h at 300 °C under vacuum, (ii) HMITFSI was dissolved in methanol (99.9%), (iii) the zeolite powder was added to the solution forming suspensions with six different HMITFSI/NaY weight ratios, namely IL/Z = 0.03, 0.05, 0.1, 0.2, 0.5, and 1, and (iv) the suspension was heated at 90 °C to evaporate the solvent overnight and was then heat treated at 230 °C for ~8 h. The entire procedure was carried out in a glove bag filled with Ar.

### 2.2. Characterization

Powder X-ray diffraction (XRD) patterns were obtained on a Bruker D-8 ADVANCE diffractometer equipped with a LynxEye position sensitive detector, using a Cu Kα X-ray source (40 kV, 40 mA).

The textural properties of the composites were determined by nitrogen physisorption experiments carried out at −196 °C using a Quantachrome Autosorb-1 Series Surface Area and Pore Size Analyzer. The total and the micropore surface area were calculated following the BET (Brunauer–Emmett–Teller) procedure and *t*-plot method, respectively. The samples, prior to the measurements were outgassed at 200 °C for 3 h under vacuum.

Thermogravimetric analysis (TGA) was performed using a Q50 TGA apparatus (TA Instruments, Inc.). The amount of ionic liquid in each composite was verified by recording the weight loss when the samples were heated from room temperature to 650 °C under flowing Ar with a heating rate 5 °C min$^{-1}$. The water adsorption capacity of each sample was also estimated using the following procedure: (i) each sample was outgassed at 200 °C under the flow of dry Ar and its weight was recorded; (ii) the feed was switched from dry Ar to Ar with ~4.2 kPa of $H_2O$ vapours; (iii) the sample temperature was adjusted to the desired value (150 °C, 120 °C, and 80 °C), (iv) at each temperature the weight was recorded once equilibration was achieved; and (v) the % weight changes (dw%) were calculated using the equation $dw\% = [(W_i - W_0)/W_0)]100$, where $W_i$ is the weight of the sample after equilibration with water vapours and $W_0$ the weight of the outgassed sample at 200 °C.

FT-Raman spectra were acquired using a Bruker (D) FRA-106/S component attached to an EQUINOX 55 spectrometer. A R510 diode pumped Nd:Y AG laser at 1064 nm operating at 250 mW was used for Raman excitation. The samples were pressed into a stainless steel holder and the spectra were recorded using 4 cm$^{-1}$ resolution and 800 scans.

The conduction properties of the samples were evaluated using A.C. impedance spectroscopy. The measurements were carried out

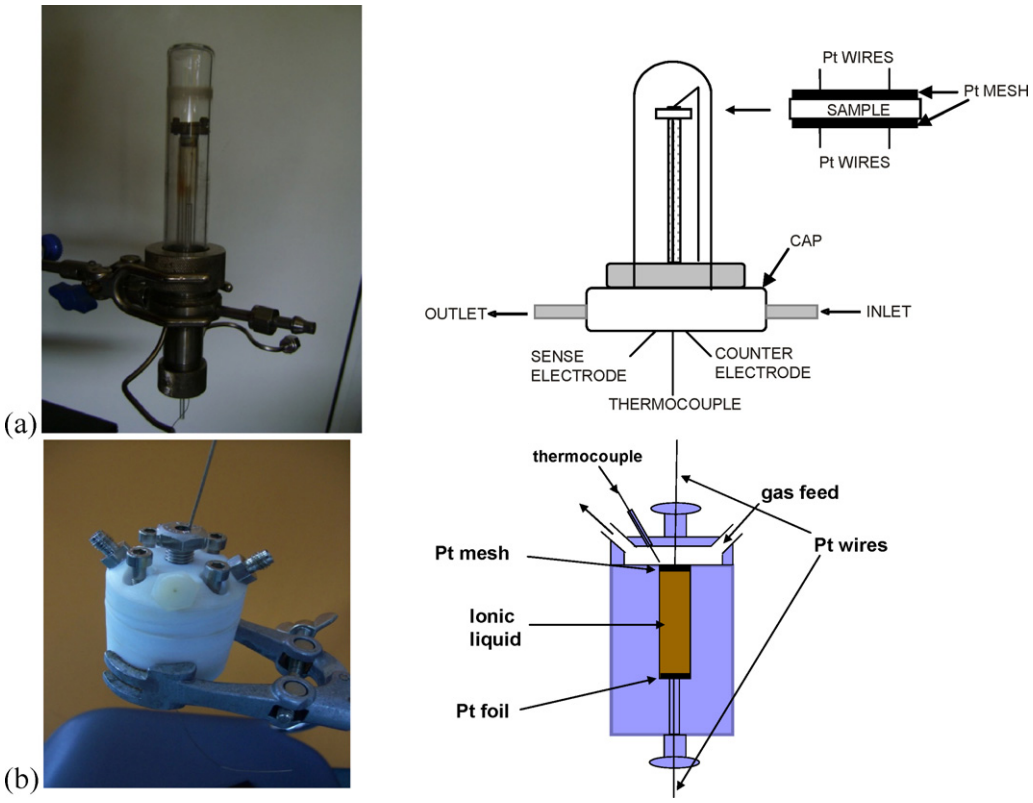


**Fig. 1.** Schematic representations and photographs of the homemade cells used for the electrochemical measurements of the composites (a) and the ionic liquid (b).

using an Autolab PG302 potentiostat–galvanostat connected to an Autolab FRA2 frequency response analyzer module. The frequency was varied from 10 mHz to 100 kHz. The Nyquist diagram that was obtained allowed the calculation of the resistance value by the point at which the semicircle plotted for high frequencies and the inclined line for low frequencies meet [23]. The conductivity values were calculated using the following equation: $\sigma = (1/R)\,(l/S)$, where $\sigma$ is the conductivity ($S\,cm^{-1}$), $R$ is the resistance (ohm), $l$ is the sample thickness (cm) and $S$ the contact surface with the electrodes ($cm^2$).

The experiments were carried out by measuring the through plane conductivity of two electrode pellets. The pellets (diameter ~14 mm, thickness ~1.35 mm) were prepared using the following procedure: The powders (90% of the sample and 10% poly-vinylidene fluorine (PVDF) polymer that acts as a binder) were pressed using a stainless steel press at 5 t for 1 min. A gold layer was also sputtered on both sides in order to ensure a continuous electrochemical interface between the sputtered Au film and the pellet. The pellets were placed in a homemade cell (Fig. 1a). The conduct electrodes to the Au sputtered film are made of Pt mesh and are connected to external electric circuit through Pt wires. The measurements were carried out as a function of temperature in dry atmosphere as well as in the presence of ~4.2 kPa of water vapours. The conductivity of HMITFSI was also measured in the same conditions using a different cell (Fig. 1b). This cell was made of Teflon and the electrodes were made of Pt.

SEM images of the gold-coated pellets were acquired using a LEO-SUPRA 35VP Field Emission Scanning Electron Microscope operated at 5 kV in the high vacuum mode.

### 2.3. Modelling

The analogy between ion conduction and electrical conduction from the viewpoint of the transport equation that describes both processes in the absence of convection allows the employment of the Effective Medium Theory for the calculation of the effective conductivity in blends of materials with different conductivities.

For three-dimensional dispersions of spheres Bruggeman [24] arrived at the equation:

$$(1-\varepsilon)\frac{\sigma-\sigma_e}{\sigma+2\sigma_e}+\varepsilon\frac{\sigma_b-\sigma_e}{\sigma_b+2\sigma_e}=0 \quad (1)$$

where $\sigma_e$ stands for the effective conductivity, $\sigma_b$ is the conductivity of the medium, $\sigma$ is the conductivity of the obstacles, and $\varepsilon$ is the porosity. Kirkpatrick [25] performed a similar analysis on random networks of electrical resistors in two and three dimensions.

Later, Burganos and Sotirchos [26] proved that application of EMT in pore or resistor networks leads to effective, homogenized media that satisfy the Smooth Field Approximation, which facilitates considerably the calculation of the effective conductivity, in contrast to the original, heterogeneous networks.

The Effective Medium Theory can be used to relate the grain (zeolite filled with ionic liquid) conductivity with the granular system conductivity. In fact, given that the effective conductivity of the granular medium can be measured experimentally, one can use the EMT equation to extract the grain conductivity. This is a valuable quantity that could not be measured experimentally in a direct manner. To this end, Eq. (1) can be used with $\sigma_b = 0$ (interstitial space is non-conducting). Thus,

$$\sigma_{ZL}=\frac{2}{2-3\varepsilon}\sigma_e \quad (2)$$

where $\sigma_{ZL}$ stands for the conductivity of the zeolite grain containing some quantity of ionic liquid. Eq. (2) is obviously valid under the assumption that the majority of the ionic liquid is adsorbed in the interior of the zeolite grains. This is true for ionic liquid loadings that are below a threshold value, above which a non-negligible portion of the liquid is dispersed in the intergranular region.

For ionic liquid loadings higher than the aforementioned threshold, gradually increasing portions of the void phase are occupied by

**Table 1**
Textural properties of NaY and the composites.

| IL/Z | BET area ($m^2\ g^{-1}$)[a] | Micropore volume ($cc\ g^{-1}$)[b] | Micropore area ($m^2\ g^{-1}$)[b] | External surface area ($m^2\ g^{-1}$)[b] | Total pore volume ($cc\ g^{-1}$) |
|---|---|---|---|---|---|
| NaY | 505.3 | 0.2595 | 493.3 | 13.01 | 0.2833 |
| 0.03 | 471.1 | 0.2431 | 461.4 | 9.68 | 0.2652 |
| 0.05 | 467.6 | 0.2374 | 453.9 | 13.62 | 0.2609 |
| 0.1 | 383.7 | 0.1955 | 372.4 | 11.25 | 0.2180 |
| 0.2 | 264.2 | 0.1318 | 251.3 | 12.90 | 0.1562 |
| 0.5 | 2.0 | 0 | 0 | 2.00 | 0.1548 |
| 1 | 1.1 | 0 | 0 | 1.10 | 0.0084 |

[a] Multipoint BET.
[b] *t*-Plot method.

ionic liquid rendering the material a three-phase system, each of which having a different conductivity. In this case, direct application of the EMT equation would give

$$\zeta_Z \frac{\sigma_{ZL} - \sigma_e}{\sigma_{ZL} + 2\sigma_e} - \frac{\varepsilon}{2} + \zeta_L \frac{\sigma_L - \sigma_e}{\sigma_L + 2\sigma_e} = 0 \quad (3)$$

where $\zeta_Z$ is the volume fraction of the zeolite grains, $\zeta_{ZL}$ is the volume fraction of the free ionic liquid (that is, outside the zeolite grains), and $\sigma_L$ is the conductivity of the ionic liquid. Note that the conductivity of the void phase is set equal to zero in Eq. (3).

The main assumptions behind Eq. (3) are that the three phases are randomly distributed in space and that the material is sufficiently rich in conducting phases to ensure the existence of conducting pathways across the material. However, during sample preparation it has been observed that the ionic liquid exhibits a preferential wettability on the zeolite grains. In this case, it can be organized in large "islands" that engulf the zeolite grains. If it is assumed that these islands are sufficiently large to justify the application of EMT at the scale of the islands, an effective conductivity of the islands can be obtained from the EMT equation,

$$\zeta_Z \frac{\sigma^0_{ZL} - \sigma_{e,I}}{\sigma^0_{ZL} + 2\sigma_{e,I}} + \zeta_L \frac{\sigma_L - \sigma_{e,I}}{\sigma_L + 2\sigma_{e,I}} = 0 \quad (4)$$

where $\sigma_{e,I}$ is the effective conductivity of the islands and $\sigma^0_{ZL}$ is the conductivity of the zeolite grains saturated with ionic liquid. As a second step, one can view the material as a two-phase system, made up of islands (homogenized thanks to the application of EMT at that scale) that are dispersed in a medium of zero conductivity. Hence, the effective conductivity of the material can be obtained from the EMT equation for a two-phase system, leading to

$$\sigma_e = \frac{2 - 3\varepsilon}{2} \sigma_{e,I} \quad (5)$$

This two-step EMT approach is expected to provide an improved description of the conduction phenomena in the interior of the material and offer effective conductivity estimates that are significantly higher than those predicted under the assumption of completely random distribution of the ionic liquid phase in the intergranular space.

If the ionic liquid/zeolite mass ratio, $\omega$, is known, the volume fraction of the zeolite grains can be found from the following relationship

$$\zeta_Z = \frac{1 - \varepsilon}{1 + \frac{\rho_Z}{\rho_L}(\omega - \omega^0)} \quad (6)$$

where $\rho_Z$ and $\rho_L$ are the densities of the zeolite and of the ionic liquid, respectively, $\omega$ is the ionic liquid to zeolite mass ratio, and $\omega^0$ is the value of $\omega$ at which the zeolite grains are saturated with ionic liquid. For $\omega > \omega^0$ the ionic liquid resides also in the intergranular space in addition to the amount that is adsorbed within the grains. Notice that for $\omega = \omega^0$, Eq. (6) reduces to $\zeta_Z = 1 - \varepsilon$, as expected following elimination of the ionic liquid that resides outside the zeolite grains.

Information about the porosity of the material can be extracted either from the SEM pictures (following appropriate digitization and image processing) or from the intrusion part of the mercury porosimetry curves. Both of these techniques were used here and presented only small deviations from each other, which is expected from the fact that SEM gives information about the entire porosity whereas mercury porosimetry gives only the accessible porosity. The value of $\zeta_L$ can be obtained from

$$\zeta_Z + \varepsilon + \zeta_L = 1 \quad (7)$$

## 3. Results & discussion

### 3.1. $N_2$ physisorption

Table 1 shows the textural properties of each sample calculated using the $N_2$ physisorption isotherms shown in Fig. 2a. Both BET, micropore area and pore volume decrease progressively with the HMITFSI loading. The micropore surface area, normalized with respect to the total mass of the sample and to the mass of zeolite, as a function of HMITFSI loading is shown in Fig. 2b. When normalization is carried out with respect to zeolite weight slightly higher values were obtained. The graphs indicate that the pores are completely filled when the IL/Z ratio is around 0.5. This observation can be attributed either to the formation of an HMITFSI layer on the external surface of the zeolite that essentially blocks the access of $N_2$ to the "interior" volume of the crystal or to the gradual fill of the entire zeolite pore volume. If the former explanation was true, then the micropore volume should have been essentially loading independent until the external surface of the zeolite crystals was completely covered. Then an abrupt decrease of the micropore volume should have been observed once the amount of HMITFSI was enough to completely cover the entire external (geometric) surface area of the crystals. Thus, the gradual decrease of the specific surface area shown in Fig. 2b is indicative of the zeolite pore filling with HMITFSI.

### 3.2. X-ray diffraction

The recorded XRD patterns of the NaY and HMITFSI/NaY composite with IL/Z = 1 are presented in Fig. 3. The XRD patterns of NaTFSI, HMITFSI and the rest of the HMITFSI/NaY composites are presented as supporting information (Figs. S1 and S2). The characteristic peaks of NaY are clearly present in the spectra of all composites, indicating that the encapsulation procedure did not destroy the zeolite framework. New diffraction peaks can be seen in the spectra of the samples with IL/Z = 0.2, 0.5 and 1. These peaks are characteristic of NaTFSI. This observation clearly shows that the entrapment of HMITFSI was also accompanied by an ion-exchange reaction. Taking into account that the Si/Al ratio of the zeolite crystals used in this work is ~2.8, the following two reactions can be

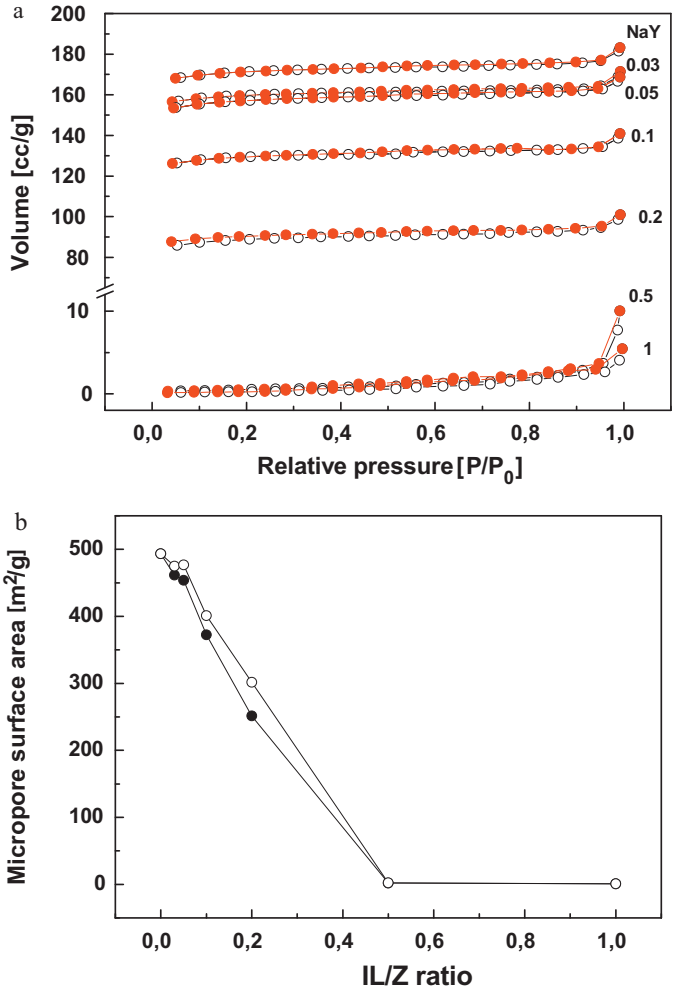


**Fig. 2.** (a) $N_2$ physisorption isotherms of NaY and HMITFSI/NaY composites. (The numbers denote the IL/Z of each sample) (b) micropore surface area vs. IL/Z ratio ((○): per zeolite mass, (●): per sample mass).

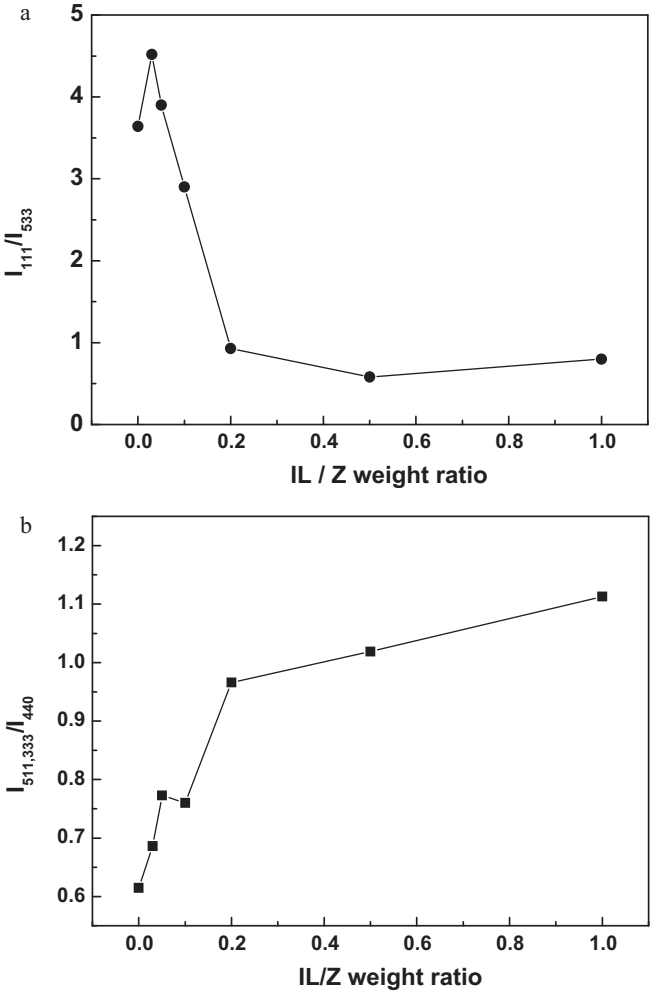


**Fig. 4.** XRD intensity ratios $I_{111}/I_{533}$ (a) and $I_{511,333}/I_{440}$ (b) vs. IL/Z.

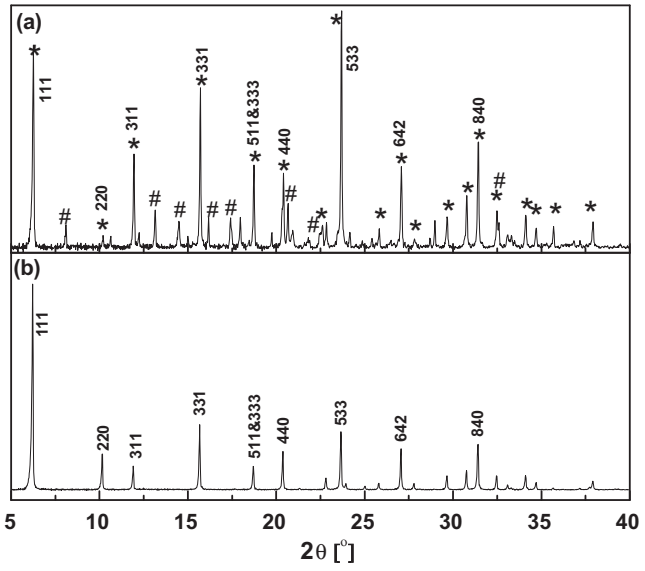


**Fig. 3.** XRD spectra of (a) NaY and (b) HMITFSI/NaY composite with IL/Z = 1 (*: NaY and #: NaTFSI).

considered as possible:

$$Na_{50.5}Si_{141.5}Al_{50.5}O_{384} + yHMITFSI \leftrightarrow HMI_yNa_{(50.5-y)}Si_{141.5}Al_{50.5}O_{384} + yNaTFSI \quad (R1)$$

or

$$Na_{50.5}Si_{141.5}Al_{50.5}O_{384} + yHMITFSI \leftrightarrow H_yNa_{(50.5-y)}Si_{141.5}Al_{50.5}O_{384} + yNaTFSI + yMI \quad (R2)$$

Furthermore, the following differences between the relative intensities of the X-ray diffraction peaks of NaY are observed: 1. The intensity ($I$) of the 1 1 1 reflection (at ~6.2°) decreases with HMITFSI loading. As a result, in the samples with IL/Z = 0.5 and 1 the (5 3 3) reflection has the highest intensity (Fig. 4a). 2. The relative intensities of the 5 1 1/3 3 3 and 4 4 0 reflections change. As the HMITFSI increases $I_{440}$ becomes higher than $I_{511/333}$ (Fig. 4b). 3. Differences between the relative order of the peak intensities of the (2 2 0), (3 1 1) and (3 3 1) reflections of the composites and of NaY can be identified. In NaY (and the composites with IL/Z = 0.03 and 0.05) the following relation is satisfied: $I_{331} > I_{220} > I_{311}$. In the composite with IL/Z = 0.1: $I_{220} \approx I_{311}$, while in the composites with IL/Z = 0.2, 0.5, and 1: $I_{331} > I_{311} > I_{220}$. Similar observations have been reported for $Fe^{II}(bpy)_3$ [27] and for organic [28] or metallorganic complexes entrapped into NaY [29–32] and they have been attributed to a re-distribution of $Na^+$ ions into the zeolite crystal. The observed changes can also be attributed to the X-ray scattering by the encapsulated HMITFSI molecules [33] and to the exchange of the extra

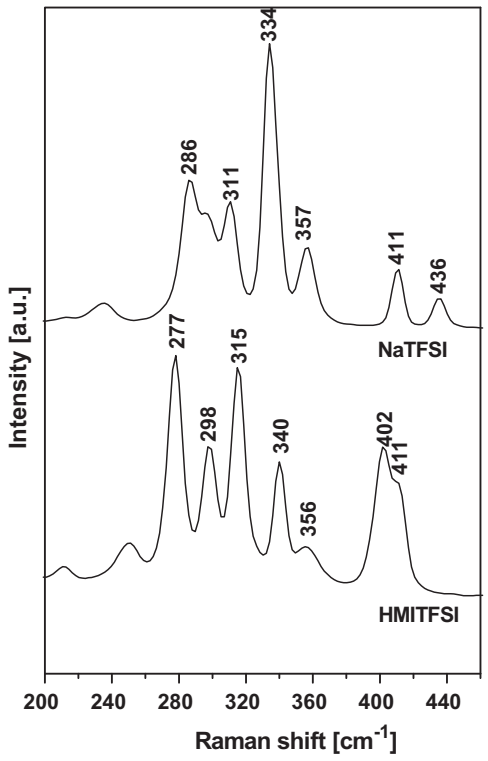


**Fig. 5.** FT-Raman spectra of HMITFSI and NaTFSI between 260 and 460 $cm^{-1}$.

framework $Na^+$ with $HMI^+$. Both of these explanations provide strong indication for the presence of $HMI^+$ inside the NaY pores.

It is interesting to note that the changes of the zeolite XRD patterns at IL/Z ratios less than 0.2 are not accompanied by the observation of any reflections attributed to NaTFSI. This indicates that either the amount of NaTFSI formed is below the detection limit of our method or that NaTFSI forms clusters that are too small to show any diffraction peaks. It is not possible to distinguish whether such clusters can be located either in the zeolite pores or on the zeolite external surface area.

### 3.3. FT-Raman measurements

The FT-Raman spectra of HMITFSI, NaTFSI and NaY and their assignments are shown as the supporting information (Fig. S3 and Table S1 respectively). The analysis of the vibrational spectroscopy spectra can provide information about the conformation of the HMITFSI ions before and after encapsulation. It is known from previous studies that the $TFSI^-$ can be found either in the cis or trans conformation, which are often called $C_1$ and $C_2$, respectively [34]. Furthermore, it is possible for $HMI^+$ to lose its proton and become neutral [35]. The anion of NaTFSI is known to obtain the cis conformation [36] and its FT-Raman spectra will be used as reference for the understanding of the spectra of HMITFSI.

The region of the FT-Raman spectra in the case of NaTFSI and HMITFSI between 200 and 460 $cm^{-1}$, shown in Fig. 5, has been suggested to be particularly suitable for analyzing the conformations of $TFSI^-$ because the bands due to imidazole cation in this spectral region are rather weak [35,37]. Zak et al. [36] report that the structures of $HN(SO_2R)_2$ with R = F, $CF_3$ adopt trans conformation while in the case of their salts with $Na^+$ and in general with alkali metal cations the anion adopts the cis conformation due to their extensive coordination with oxygen atoms. The bands in the case of NaTFSI at 286, 311, 334, and 357 $cm^{-1}$ as well as the pair at 411 and 435 $cm^{-1}$ are indeed characteristic of the cis conformation of the anion [37]. On the other hand, the spectra of HMITFSI in this region exhibit

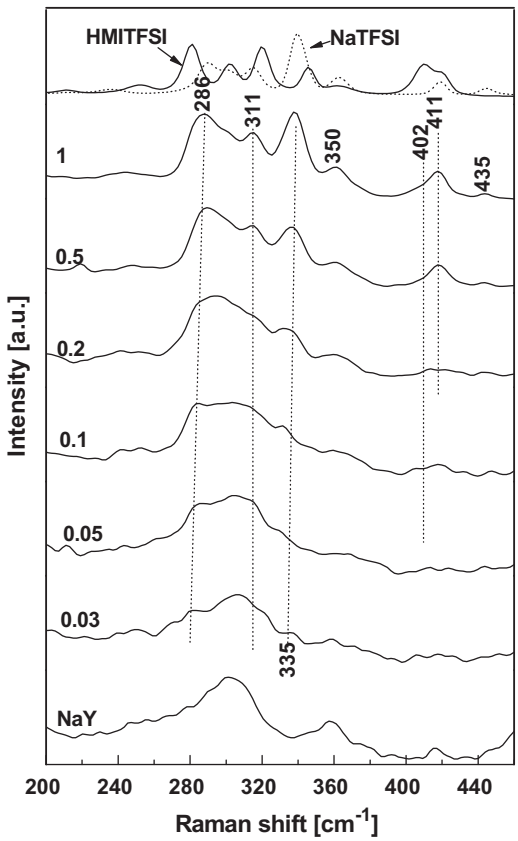


**Fig. 6.** Comparison of the FT-Raman spectra of composites between 200 and 460 $cm^{-1}$ with those of NaY, HMITFSI and NaTFSI.

bands at 277, 298, 315, and 340 $cm^{-1}$ and at 402 and 411 $cm^{-1}$ which are characteristic of the $TFSI^-$ trans conformer [37].

The FT-Raman spectra of the composites between 200 and 460 $cm^{-1}$ are shown in Fig. 6. With increasing the HMITFSI loading, the Raman spectra show systematic changes. New bands are superimposed on the broad band centred at about 303 $cm^{-1}$ that is attributed to NaY. Their intensity increases with the amount of HMITFSI. The bands observed for the composite with IL/Z = 1 are similar to those of NaTFSI. This observation is in agreement to the conclusions from the X-ray diffraction data. The existence of a band at 402 $cm^{-1}$ indicates the presence of HMITFSI as well.

### 3.4. TGA measurements

The TGA measurements were performed for all the composites and confirmed the nominal loading of the ionic liquid. The mass fraction of $H_2O$ adsorbed, normalized to the initial mass of zeolite, as function of HMITFSI loading, at three different temperatures is shown in Fig. 7. The amount of $H_2O$ adsorbed decreases with temperature and with HMITFSI loading approaching a plateau value at high loadings (IL/Z = 0.5). For example, the sample with IL/Z = 1 adsorbs about 5 times less water compared to pure NaY. Experiments carried out using HMITFSI indicated that it does not absorb water at the temperature range studied. As a result, the observed decrease in water adsorption capacity can be attributed to the zeolite pore filling from the HMITFSI molecules. The above results are in accordance with the textural properties shown in Fig. 2 that indicate the filling of the NaY pores.

### 3.5. Conductivity measurements

The conductivity of NaY in dry atmosphere is compared to values reported in the literature [3,4] in Fig. 8. In all cases, it increases with

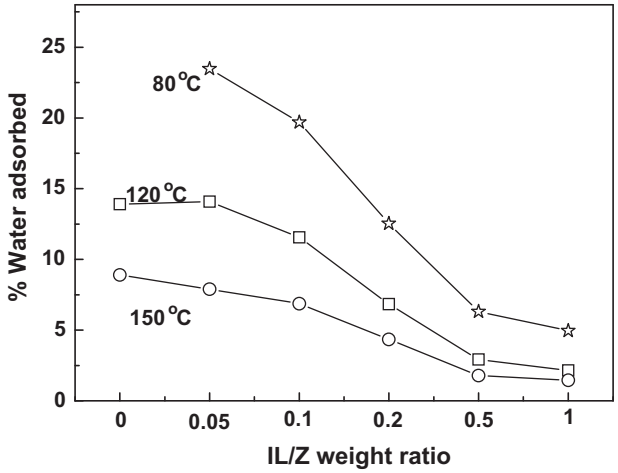


**Fig. 7.** Weight fraction of water uptake vs. IL/Z weight ratio at 80, 120 and 150 °C.

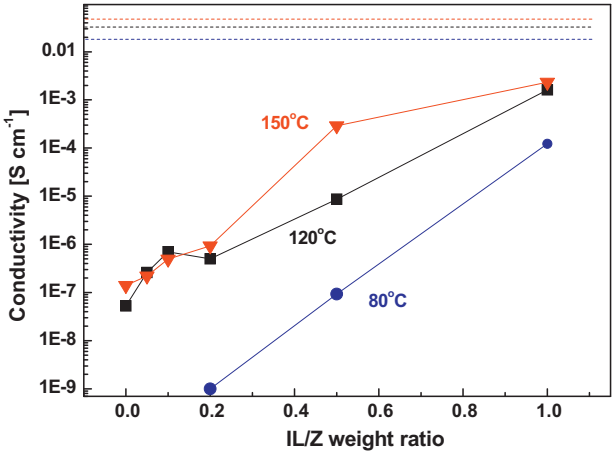


**Fig. 9.** Conductivity of the composites as a function of IL/Z at 80, 120 and 150 °C under dry atmosphere. The dotted lines show the conductivity of HMITFSI at 80, 120 and 150 °C.

temperature. However, the values measured in this work are higher than those previously reported. Freeman et al. have attributed the increase of conductivity with temperature to the enhancement of the zeolite extra framework $Na^+$ mobility [3]. The differences between the values measured and the previously reported values can be attributed either to differences of the Si/Al ratio of the FAU crystals used, to the presence of residual humidity, or to the porosity of the NaY pellets. The macropore porosity of the NaY pellets used in the previous studies was ~10–13%, while in our case it is estimated between 18 and 22%. Higher macropore porosity, should result in a decrease of the measured conductivity. The Si/Al ratio of the crystals used in our study (~2.8) was higher than that of the crystals used by Freeman and Stamires [3] and by Abdoulaye et al. [4] (~2.6, and 2.5 respectively) indicating that a lower number of sodium cations per unit cell can contribute to conductivity. The pellets used in our study were degassed at 150 °C prior to conductivity measurements, while in the previous studies at 400 °C. The lower dehydration temperature, which has been selected due to the presence of the PVDF binder, might not have been high enough to achieve complete dehydration of the NaY crystals. Stamires [5] showed that the conductivity of zeolites X and A increases with the number of adsorbed water molecules. Based on the above, the higher values of NaY conductivity can be attributed primarily to the contribution of traces of humidity.

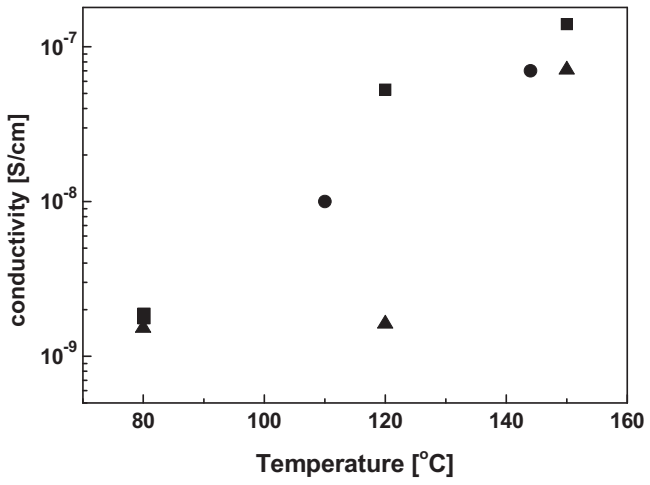


**Fig. 8.** Comparison of NaY pellet conductivity (■) as a function of temperature to the values from references 3 (●) and 37 (▲).

The conductivity of the composites in dry atmosphere against the HMITFSI loading at 80, 120 and 150 °C is shown in Fig. 9. At all temperatures it increases with IL/Z ratio. The conductivity of the composite with IL/Z = 1 at 150 °C is ~4 orders of magnitude higher than that of NaY powder and about one order of magnitude lower to that of pure HMITFSI. It must be pointed out, that the data shown are indicative of the overall motion of all ions and does not necessarily correspond to proton conductivity. However, earlier studies have shown that $H^+$ conduction through a similar protic ionic liquid (Him TFSI) can take place through a vehicle type mechanism or/and through a Grotthuss type mechanism [38]. In a vehicle type of mechanism protons migrate attached to larger molecules (i.e. $H_3O^+$, $HMI^+$, etc) which are the "vehicles". As a result, the molecular diffusion of the "vehicle" determines conductivity. In the case of a Grotthuss mechanisms, protons are transferred from one "vehicle" to the next one (proton donor–proton acceptor). This transfer can occur via the formation of hydrogen bonds. However, in order to create a percolating path for proton transfer a reorientation–reorganization of the proton carriers is frequently required. As a result, in the case of a Grotthuss type mechanism, conductivity depends on the proton transfer and on the proton carrier reorientation rates. In our case both ions of the HMITFSI can be considered as proton carriers. A proton can bind to $TFSI^-$ forming HTFSI which is a strong acid with relatively low intermolecular proton transfer ability. As a result, the $TFSI^-$ is expected to contribute primarily to the "vehicle" transport mechanism. On the other hand, $HMI^+$ can contribute to proton transfer through both mechanisms.

The experimental measurements of the conductivity of pelletized zeolite/ionic liquid samples presented in Fig. 9 in combination with the characterization results (Figs. 2–4 and Figs. S1–S4) suggest that for ionic liquid/zeolite mass ratio lower than 0.2 the majority of the ionic liquid resides in the interior of the zeolite grains. Hence, one may use as an approximate estimate of the threshold value for the mass ratio the value $\omega^0 = 0.2$. The precise value of $\omega^0$ was not found to affect, essentially, the model predictions except for a small shift of the steep part of the EMT curve (see next section). Below this level, the free ionic liquid is negligible and one can use the experimental measurements of the pellet conductivity to extract the conductivity of the zeolite grain from Eq. (2). Using the porosity value from the mercury porosimetry analysis ($\varepsilon = 0.18$–$0.22$ depending on the ionic liquid loading), the zeolite grain conductivity is estimated to take values approximately twice as high as the pellet conductivities. This estimate can then be used to calculate the pellet conductivity for ionic liquid

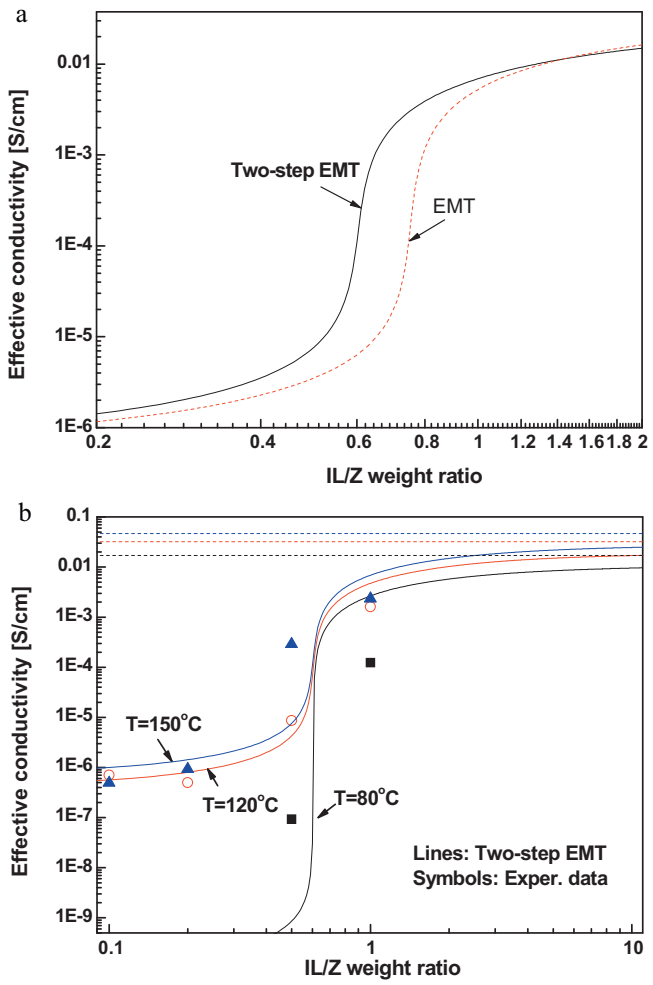


**Fig. 10.** (a) Comparison of the predictions of the single step EMT equation with those of the two-step EMT approach for ionic liquid/zeolite pellet conductivities at 150 °C above the threshold value at which free ionic liquid appears (b) Effective conductivity vs. ionic liquid/zeolite mass ratio using the two-step EMT approach at three different temperature values. Comparison with experimental data.

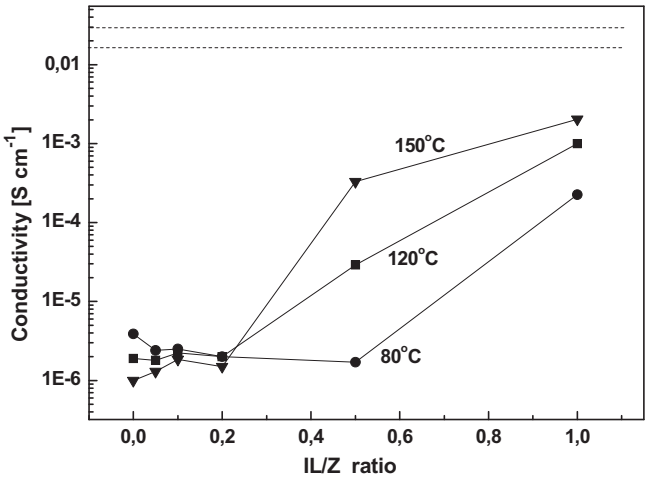


**Fig. 11.** Conductivity of the composites as a function of IL/Z ratio at 80, 120 and 150 °C under the presence of 4.2 kPa of water vapours. The dotted lines show the conductivity of HMITFSI at 80 and 120 °C.

loadings higher than the threshold value and allow the investigation of the dependence of the pellet conductivity on the loading for all temperature values examined in this work.

Fig. 10a provides a comparison between the predictions of the single step EMT equation, which assumes a random distribution of the free ionic liquid in the intergranular space, to the predictions of the two-step EMT approach that is suggested in this work as more suitable to capture the fact that the free ionic liquid wets the zeolite grains and forms "islands" of liquid engulfing the grains. It is apparent that the two-step EMT approach leads to much higher estimates of the pellet conductivity than the direct application of the EMT equation, by 1–2 orders of magnitude for ionic liquid/zeolite mass ratio between 0.6 and 0.8. This reveals the strong effect of the phase distribution in these systems and, more specifically, of the organization of the free ionic liquid in the intergranular space, on the conductivity of the material.

The two-step EMT approach will be used for the comparison with the experimental measurements of the pellet conductivity for all three temperature values examined in this work and for the investigation of the role of the ionic liquid loading on the conductivity of the material. Fig. 10b shows that the two-step EMT approach follows quite satisfactorily the conductivity measurements for all three temperature values and appears to capture quantitatively the sharp increase of the conductivity right above the threshold value $\omega^0 = 0.2$. Note that the density values for the ionic liquid and the empty zeolite that are needed in Eq. (6) were taken from the literature [39] and that no adjustable parameter was employed in the calculations. The deviation that is observed in some cases is attributed to the fact that the EMT approximation assumes infinitely large systems in addition to the requirement of loadings that are clearly larger than the percolation threshold. The former assumption requires a very large correlation length of the ionic liquid/zeolite islands, which is not ensured here. In addition, the model neglects potential ion-exchange phenomena between the ionic liquid and the framework, which might lead to sodium cations residing outside the zeolite grains and, hence, alter the interstitial conductivity.

The conductivity of all samples measured in the presence of ~4.2 kPa of water vapours is shown in Fig. 11. The conductivity of NaY powder (IL/Z = 0) is higher than that measured at dry conditions. However, it decreases with increasing temperature. According to Stamires [5] the presence of adsorbed water decrease the cation binding energy to the zeolite lattice with a concomitant increase of their mobility providing an explanation to the observed conductivity enhancement. As shown by the TGA measurements (Fig. 7), the amount of adsorbed water molecules decreases with increasing temperature (at constant water vapour partial pressure). As a result, the effect of temperature on NaY conductivity can be attributed to the reduction of the number of adsorbed water molecules. It is also seen that at 80 °C, conductivity decreases with HMITFSI loading up to IL/Z ~ 0.5 followed by a sharp increase at higher loadings. At 120 °C, conductivity was essentially not affected by HMITFSI loading up to IL/Z ~ 0.2, while at 150 °C only a slight increase was observed up to IL/Z ~ 0.2. Higher ratios of IL/Z resulted in a sharp increase of conductivity at all temperatures. If the amount of ionic liquid added is smaller than that required to complete fill the zeolite pores, then conduction can take place due to the presence of adsorbed water and of ionic liquid molecules. As the IL/Z ratio increases, the NaY micropore pore volume, and water adsorption capacity decreases (Figs. 2 and 7) As a result, the encapsulation of HMITFSI seems to have a dual role in the conductivity measurements in the presence of water vapours. It enhances conductivity by providing a new path and it reduces the contribution of adsorbed water to conductivity. The latter can occur either through the reduction of water adsorption capacity and/or through the blocking of the solvated cation motion. At high IL/Z values (IL/Z > ~0.2) a sharp increase of conductivity with loading is observed. For example, the conductivity of the sample with IL/Z = 1 is about 3 orders

of magnitude higher than that of pure zeolite despite the relatively low water uptake (~5% of its weight, according to the TGA). This result indicates that at samples with high IL/Z conduction is similar to that under dry conditions. Notice that direct comparison with model predictions is not possible in the presence of humidity due to the lack of data for the conductivity of the zeolite framework as a function of the amount of adsorbed water molecules, which is further complicated by the fact that the precise amount of sorbed water within the zeolite is affected by the penetration of ionic liquid into the micropore system.

## 4. Conclusions

The physicochemical properties of H-3-methyl imidazolium bis(trifluoromethanesulfonyl) imide/NaY composites were determined using XRD, $N_2$ physisorption, FT-Raman, TGA and A.C. impedance spectroscopy. Our results strongly denote that the entrapment of HMITFSI into the NaY framework is accompanied by an ion exchange reaction that takes place between the ions of the ionic liquid and the sodium ions of the zeolite framework. The XRD patterns of the composites exhibit changes of the peak intensities that denote that $Na^+$ are replaced by $HMI^+$. The formation of NaTFSI is also confirmed by the FT-Raman spectra of the composites. In particular, the $TFSI^-$ anions in the composites, adopts the cis conformation as in NaTFSI instead of the trans conformation that is dominant in HMITFSI. As the loading in IL of the composites increases the water capacitance decreases as a consequence of the decrease of the micropore surface area. The A.C. impedance measurements showed that the conductivity of the composites, at dry conditions increase with loading and temperature. A sharp enhancement was observed when the IL fraction was higher than 0.2. Measurements at wet conditions ($P_{H_2O}$ = 4.2 kPa) revealed two different temperature dependencies. At low IL loadings ($x_{IL} < 0.2$) the conductivity decreased with increasing temperature while the opposite occurred at higher IL loadings. This observation can be attributed to the contribution of two competing mechanisms (transport through hydrated sites & transport due to the IL). Moreover, theoretical calculations were performed. The ionic liquid/zeolite island configuration that was suggested by the SEM images of pelletized samples of the material stimulated the development of a two-step EMT approach for the prediction of the conductivity of the material as a function of the ionic liquid loading. The predictions compared quite satisfactorily with the experimental measurements despite the significant uncertainty regarding the details of the phase organization at the mesoscopic scale. The model shows a sharp increase of the conductivity right above a critical threshold value for the ionic liquid/zeolite mass ratio, followed by a more moderate increase at higher loadings.

## Acknowledgements

The authors would like to acknowledge financial support from the European Commission through the FP7 funded program ZEOCELL (Grant Agreement no: 209481) and the Solvionic S.A. for providing the HMITFSI and NaTFSI.

## Appendix A. Supplementary data

Supplementary data associated with this article can be found, in the online version, at doi:10.1016/j.jpowsour.2010.09.061.

## References

[1] Q. Li, J.O. Jensen, R.F. Savinell, N.J. Bjerrum, Prog. Polym. Sci. (Oxford) 34 (2009) 449.
[2] E.K. Pefkianakis, V. Deimede, M.K. Daletou, N. Gourdoupi, J.K. Kallitsis, Macromol. Rapid Commun. 26 (2005) 1724.
[3] D.C. Freeman Jr., D.N. Stamires, J. Chem. Phys. 35 (1961) 799.
[4] A. Abdoulaye, S.S. Soulayman, G. Chabanis, J.C. Giuntini, J.V. Zanchetta, Micropor. Mater. 8 (1997) 63.
[5] D.N. Stamires, J. Chem. Phys. 36 (1962) 3174.
[6] J.C. McKeen, Y.S. Yan, M.E. Davis, Chem. Mater. 20 (2008) 3791.
[7] J.C. McKeen, Y.S. Yan, M.E. Davis, Chem. Mater. 20 (2008) 5122.
[8] R. Marschall, I. Bannat, J. Caro, M. Wark, Micropor. Mesopor. Mater. 99 (2007) 190.
[9] Y.F. Lin, C.Y. Yen, C.C.M. Ma, S.H. Liao, C.H. Lee, Y.H. Hsiao, H.P. Lin, J. Power Sources 171 (2007) 388.
[10] J.D. Halla, M. Mamak, D.E. Williams, G.A. Ozin, Adv. Funct. Mater. 13 (2003) 133.
[11] L.A. Banchard, D. Hancu, E.J. Beckman, J.F. Brennecke, Nature 399 (1999) 28.
[12] P. Wasserscheid, T. Welton, Ionic Liquids in Synthesis, Wiley-VCH, Mannheim, 2003.
[13] D. Zhan, M. Wu, Y. Kou, E. Min, Catal. Today 2654 (2002) 1.
[14] H. Ohno, Electrochemical Aspects of Ionic Liquids, John Wiley & Sons Inc., New Jersey, 2005.
[15] M.A.B.H. Susan, A. Noda, S. Mitsushima, M. Watanabe, Chem. Commun. 9 (2003) 938.
[16] H. Nakamoto, M. Watanabe, Chem. Commun. (2007) 2539.
[17] C. Iojoiu, M. Martinez, M. Hanna, Y. Molmeret, L. Cointeaux, J.C. Lepretre, N. El Kissi, J. Guindet, P. Judeinstein, J.Y. Sanchez, Polym. Adv. Technol. 19 (2008) 1406.
[18] H. Ye, J. Huang, J.J. Xu, N.K.A.C. Kodiweera, J.R.P. Jayakody, S.G. Greenbaum, J. Power Sources 178 (2008) 651.
[19] S.Y. Lee, T. Yasuda, M. Watanabe, J. Power Sources 195 (2010) 5909.
[20] C. DeCastro, E. Sauvage, M.H. Valkenberg, W.F. Holderich, J Catal. 196 (2000) 86.
[21] M.H. Valkenberg, C. DeCastro, W.F. Holderich, Green Chem. 4 (2002) 88.
[22] B. Pietschmann, M.A. Weiß, T. Selvam, G. Sextl, A. Gedeon, in: P. Massiani, F. Babonneau (Eds.), Studies in Surface Science & Catalysis, Elsevier, 2008, p. 325.
[23] E. Barsoukov, J.R. Macdonald, Impedance Spectroscopy, Theory, Experiment, and Applications, 2nd ed., John Wiley & Sons, Inc., 2005.
[24] D.A.G. Bruggeman, Ann. Phys 24 (1935) 636.
[25] S. Kirkpatrick, Rev. Mod. Phys. 45 (1973) 574–588.
[26] V.N. Burganos, S.V. Sotirchos, AIChE J. 33 (1987) 1678–1689.
[27] W.H. Quayle, J.H. Lunsford, Inorg. Chem. 21 (1982) 97.
[28] M. Nakayama, J. Yano, K. Nakaoka, K. Ogura, Synth. Met. 138 (2003) 419.
[29] A. Kozlov, K. Asakura, Y. Iwasawa, Micropor. Mesopor. Mater. 21 (1998) 571.
[30] M.R. Maurya, A.K. Chandrakar, S. Chand, J. Mol. Catal. A: Chem. 278 (2007) 12.
[31] R. Vijayalakshmi, S.K. Kulshreshtha, Micropor. Mesopor. Mater. 111 (2008) 449.
[32] A.H. Ahmed, A.G. Mostafa, Mater. Sci. Eng. C 29 (2009) 877.
[33] E.N. Coker, D.P. Roelofsen, R.M. Barrer, J.C. Jansen, H. Van Bekkum, Micropor. Mesopor. Mater. 22 (1998) 261.
[34] M. Herstedt, M. Smirnov, P. Johansson, M. Chami, J. Grondin, L. Servant, J.C. Lassagues, J. Raman Spectrosc. 36 (2005) 762.
[35] J. Sadlej, A. Jaworski, K. Miaskiewicz, J. Mol. Struct. 274 (1992) 247.
[36] Z. Zak, A. Ruzicka, C. Michot, Z. Kristallogr. 213 (1998) 217.
[37] J.C. Lassagues, J. Grondin, R. Holomb, P. Johansson, J. Raman Spectrosc. 38 (2007) 551.
[38] K.-D. Kruer, Chem. Mater. 8 (1996) 610–641.
[39] T.L. Greaves, C.J. Drummond, Chem. Rev. 108 (2008) 206.